2000

Influence of humidity on the aerosol scattering coefficient and its effect on the upwelling radiance during ACE-2

Gasso, S.; Hegg, D.A.; Covert, D.S.; Collins, D.; Noone, K.J.; Ostrom, E.; Schmid, B.; Russell, P.B.; Livingston, J.M.; Durkee, P.A....

Tellus (2000), 52B, 546–567
Printed in UK. All rights reserved

TELLUS
ISSN 0280–6509

Influence of humidity on the aerosol scattering coefficient and its effect on the upwelling radiance during ACE-2

By S. GASSÓ[1]*, D. A. HEGG[2], D. S. COVERT[2], D. COLLINS[3], K. J. NOONE[4], E. ÖSTRÖM[4], B. SCHMID[5], P. B. RUSSELL[6], J. M. LIVINGSTON[7], P. A. DURKEE[8] and H. JONSSON[8], [1]*Geophysics Program, Box 351650, University of Washington, Seattle, WA, USA;* [2]*Atmospheric Science Department, University of Washington, Seattle, WA, USA;* [3]*California Institute of Technology, Pasadena, CA, USA;* [4]*Department of Meteorology, Stockholm University, Stockholm, Sweden;* [5]*Bay Area Environmental Research Institute, San Francisco, CA, USA;* [6]*NASA Ames Research Center, Moffett Field, CA, USA;* [7]*SRI International, Menlo Park, CA, USA;* [8]*Naval Postgraduate School, Monterey, CA, USA*

(Manuscript received 1 March 1999; in final form 27 September 1999)

ABSTRACT

Aerosol scattering coefficients (σ_{sp}) have been measured over the ocean at different relative humidities (RH) as a function of altitude in the region surrounding the Canary Islands during the Second Aerosol Characterization Experiment (ACE-2) in June and July 1997. The data were collected by the University of Washington passive humidigraph (UWPH) mounted on the Pelican research aircraft. Concurrently, particle size distributions, absorption coefficients and aerosol optical depth were measured throughout 17 flights. A parameterization of σ_{sp} as a function of RH was utilized to assess the impact of aerosol hydration on the upwelling radiance (normalized to the solar constant and cosine of zenith angle). The top of the atmosphere radiance signal was simulated at wavelengths corresponding to visible and near-infrared bands of the EOS-AM ("Terra") detectors, MODIS and MISR. The UWPH measured σ_{sp} at 2 RHs, one below and the other above ambient conditions. Ambient σ_{sp} was obtained by interpolation of these 2 measurements. The data were stratified in terms of 3 types of aerosols: Saharan dust, clean marine (marine boundary layer background) and polluted marine aerosols (i.e., 2- or 1-day old polluted aerosols advected from Europe). An empirical relation for the dependence of σ_{sp} on RH, defined by $\sigma_{sp}(\mathrm{RH}) = k.(1 - \mathrm{RH}/100)^{-\gamma}$, was used with the hygroscopic exponent γ derived from the data. The following γ values were obtained for the 3 aerosol types: $\gamma(\mathrm{dust}) = 0.23 \pm 0.05$, $\gamma(\mathrm{clean\ marine}) = 0.69 \pm 0.06$ and $\gamma(\mathrm{polluted\ marine}) = 0.57 \pm 0.06$. Based on the measured γ's, the above equation was utilized to derive aerosol models with different hygroscopicities. The satellite simulation signal code 6S was used to compute the upwelling radiance corresponding to each of those aerosol models at several ambient humidities. For the pre-launch estimated precision of the sensors and the assumed viewing geometry of the instrument, the simulations suggest that the spectral and angular dependence of the reflectance measured by MISR is not sufficient to distinguish aerosol models with various different combinations of values for dry composition, γ and ambient RH. A similar behavior is observed for MODIS at visible wavelengths. However, the 2100 nm band of MODIS appears to be able to differentiate between at least same aerosol models with different aerosol hygroscopicity given the MODIS calibration error requirements. This result suggests the possibility of retrieval of aerosol hygroscopicity by MODIS.

* Corresponding author.
e-mail: santiago@atmos.washington.edu

1. Introduction

The determination of the direct effects of aerosols on the earth radiation balance requires quantitative information on the optical properties of atmospheric aerosols, with the more geographic resolution the better. In particular, information on the extinction properties of aerosols as a function of humidity is important (Boucher and Anderson, 1995). A recent example of this effect was shown by Hegg et al. (1997) who found that the contribution of water absorbed by aerosols off the East Coast of the United States can make up to 50% of the total aerosol optical depth. Thus, when retrieving aerosol properties such as mass concentrations from satellite detectors (Fraser et al., 1984), it is essential to have an estimation of the contribution of water to the total columnar aerosol mass. In accord with this, the direct radiative forcing by aerosols at high relative humidities ($\sim$80%) is roughly twice that of the dry aerosol (Kotchenruther et al., 1999).

The International Global Atmospheric Chemistry Project is currently addressing the issue of characterization of aerosol properties and their radiative effects by organizing a series of experiments in selected regions (IGAC, 1995). As part of this plan, the second Aerosol Characterization Experiment (ACE-2) (Verver et al., 2000) was carried out in the Canary Islands, 120 km west of Morocco, Africa, during June–July, 1997. The main goals of the experiment were to describe the radiative effects and controlling processes of aerosols, either advected from anthropogenic sources in Europe or from the Sahara desert.

Airborne data on hygroscopic growth of aerosol particles obtained with the University of Washington passive humidigraph (UWPH) during ACE-2 will be presented here. All such data were obtained onboard the ONR Pelican research aircraft. The main advantage of the UWPH is the ability to characterize aerosol hygroscopic properties with high spatial resolution (potentially one measurement every few seconds). This is accomplished by continuously and simultaneously measuring the aerosol scattering coefficient (σ_{sp}) at 2 relative humidities. From these 2 measurements (one slightly higher than ambient humidity (RH_{wet}) and the other at lower humidity (RH_{dry})), it is possible to obtain the ambient scattering coefficient (σ_{amb}) by interpolation. The retrieval of σ_{amb} has been difficult to obtain previously and is essential for closure studies of ambient columnar properties (e.g., comparison of integrated ambient scattering with aerosol optical depth derived from sunphotometer or satellite measurements).

A more general empirical characterization of the hygroscopic properties of the aerosols studied in this area is possible by deriving an aerosol hygroscopic exponent, γ, from a statistical fit of the equation (Kasten, 1969):

$$\sigma_{sp}(RH) = k(1 - RH/100)^{-\gamma} \quad (1)$$

to the measured data. The exponent γ depends on the hygroscopic nature of the aerosol and it has been shown to vary in ambient aerosols according to their chemical composition (Hänel, 1976). The accuracy of this formula has been questioned and more precise multi-parameter formulae have been suggested instead (Kotchenruther and Hobbs, 1998). Nevertheless, because of its simplicity, eq. (1) has been used in numerous calculations that require significant computer time, such as Global Climate models or satellite retrievals (Kiehl and Briegleb, 1993; Fraser et al., 1984). In this study, due to the nature of the measurements, we found a statistical fit of data to eq. (1) the most viable approach for estimation of aerosol hygroscopicity.

The retrieval of hygroscopic parameters such as γ, along with an estimation of the ambient relative humidity, will allow the determination of the water contribution to the aerosol mass and the measured total optical depth. The question of whether this contribution could be detected by satellite measurements was raised by the study of Durkee et al. (1986). They showed that variations in upwelling radiance observed by satellite detectors could be related to variations in particle size, which in turn were caused by changes in ambient relative humidity. They reached this conclusion after a study of collocated and simultaneous aerosol measurements from satellites and aircraft off the coast of Monterey, CA. However, the study focused on the retrieval of aerosol optical depth in marine environments derived from the red-visible bands of the radiometers AVHRR and CZSC (Advanced Very High Resolution Radiometer onboard of NOAA polar satellite 7 and the Coastal Zonal Scanner onboard of Nimbus 7). No attempt to derive an aerosol hygroscopic parameter was made because

of the limited spectral and angular information available from these detectors.

In light of the deployment of a new generation of satellites with much improved spatial coverage and spectral capabilities (for example, MODIS or MISR on the EOS-AM ("Terra") launched in December, 1999), it is important to assess whether the retrieval of a measure of aerosol hygroscopicity from such platforms is possible. With the help of a radiative transfer model that simulates a satellite signal (6S, Vermote et al., 1997), we examine in this paper the radiance generated by several size distributions with different degrees of hygroscopicity, all derived from the ACE-2 data set. The idea behind this procedure is to assess if typical aerosol models with different hygroscopicities have a sufficiently distinctive effect on the spectral and angular dependence of the upwelling radiance measured by such detectors to permit retrieval of aerosol hygroscopicity, specifically γ.

This paper is divided into 6 sections. We describe the instrumentation in Section 2 and the methodology used to derive the hygroscopicity data in Section 3. In Section 4, the results are presented and discussed. Section 5 is subdivided into 3 subsections: Subsection 5.1 briefly describes the model used and the satellite detector features, 5.2 discusses the adjustments and approximations made to the in-situ data used in 6S and, finally, 5.3 discusses the model results. Section 6 is dedicated to the conclusions.

2. Instrumentation

The aircraft utilized to collect the data presented in this paper was a highly modified Cessna 337 Skymaster twin-engine, centerline-thrust airframe with the forward engine eliminated. The airplane, known as "Pelican", is a long-endurance aircraft designed to perform low-altitude flights for atmospheric and oceanographic research. Some of the key features include optional onboard/remote piloting capabilities (not used during ACE-2), large payload (150 kg nose, 50 kg wings), 10- or 24-h mission capabilities (manned and unmanned missions respectively), low minimum altitude (15–30 m), reasonable ceiling ($\sim$4000 m) and low sampling speed (min $\sim$40 m/s) (Bluth et al., 1998).

The University of Washington passive humidigraph (UWPH) is an in-house design and consists of 2 nephelometers (Radiance Research, model M903, $\lambda = 0.545$ μm, Fig. 1). One of them measures the aerosol scattering coefficient at slightly below ambient relative humidity (labeled σ_{dry} throughout this paper) and the other measures the same aerosol sample at humidities above ambient (σ_{wet}). The aerosol flow is taken from the Pelican community isokinetic inlet probe which includes a small cyclone impactor with a 2.50 μm diameter (50%) aerodynamic cut-off at a nominal flow of 28 l/m. In order to avoid humidities close to 100% and thus possible condensation in the nephelometers, the air sample is heated slightly to 2°C above ambient before it is divided into the 2 nephelometers. After the split, one of the tubes goes directly to the "dry" nephelometer and the other passes through a porous Teflon tube (the "humidifier"), which was jacketed by a heated water bath before entering the "wet" nephelometer. Pre-experiment tests showed that the humidifier increased RH by 10–40% depending on ambient conditions. Both nephelometers have temperature, pressure, flow and humidity sensors. The relative humidity sensors are manufactured by Väisala

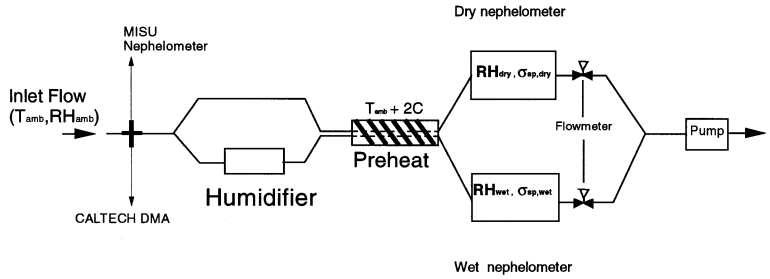

Fig. 1. Scheme of the University of Washington passive humidigraph.

(model Humiter 50U) and have a factory calibration error of 3%. A pre-campaign calibration of the nephelometers was made with particle-free air, CO_2 and Freon 134 A. During the experiment, they were recalibrated once with CO_2 and particle-free air. The detection limit was estimated at 5×10^{-6} l/m with 6 s averaging.

3. Methodology

3.1. The fit method

The derivation of the correct ambient scattering coefficient (σ_{amb}) with the statistical 2-point method assumes that scattering is a smooth function of RH between RH_{dry} and RH_{wet}, following closely the empirical eq. (1). Often the equation is an adequate model for the hygroscopic behavior of the aerosol but the accurate derivation of σ_{amb} depends critically on how far apart the wet and dry humidities are from the ambient humidity, and on the aerosol type. There is a necessary trade-off between the spatial resolution achieved with this system and the number of samples (i.e., measurements of σ_{sp} at different RHs) that can be obtained from the common inlet probe. An estimation of the conditions under which the UWPH fails to derive σ_{amb} can be obtained by comparing the fit of eq. (1) with data from a scanning nephelometer, that is, a system which continuously scans σ_{sp} as a function of controlled RH. Since this type of measurement was unavailable on the Pelican platform, we use data obtained at 2 different ground sites to illustrate this point. Figs. 2a,b show scans of the ratio $F(RH) = \sigma_{sp}(RH)/\sigma_{sp}(RH_o)$ as a function of RH for 2 contrasting aerosol types: polluted/continental sample at Sagres, Portugal measured during ACE-2 (Carrico et al., 2000) and a clean marine sample at Cape Grim, Tasmania during ACE1 (Carrico et al., 1998). In each figure, the derived γ's for all points in the ascending and descending RH scans (γ_{inc} and γ_{dec} respectively) are listed in the figure as well as 3 examples where eq. (1) was fit with 2 points. The 2 points were selected at different sections of the curve in order to reproduce the measurement conditions observed in the UWPH during the experiment.

Fig. 2a shows a clean marine aerosol with deliquescence point around 82%. Clearly the 2-point fit (indicated with filled symbols) produces significantly different γ's depending on the RH range and the part of the hygroscopic growth curve used, especially considering hysteresis. A retrieval of σ_{amb} will be approximate at best since the history of the aerosol sample is unknown (i.e., whether it had been under a regime of increasing or decreasing ambient RHs). The salt component in the sample, which results in deliquescence behavior, is the main cause of the error in the derived σ_{amb}. This does not commonly occur when sampling polluted marine aerosols with little deliquescence. For such aerosols, even a large separation between RH_{dry} and RH_{wet} still allows the derivation of σ_{amb} with low error. An example of such a case is displayed in Fig. 2b, where several 2-point fits as well as all point fits are shown. Unlike the clean case, the γ's derived from the 3 pairs of points selected are very similar to the γ's derived with all points of the scan.

3.2. Raw data and data classification

The composition of the aerosol will largely determine the value of the derived γ's, as well as the validity of the empirical eq. (1). This suggests that a stratification of γ's by aerosol composition would be useful. However, considerations of the types and frequency of the data available render direct stratification based on composition infeasible. Although the UWPH itself has reasonably high spatial resolution ($\sim$0.25 km), the concurrent airborne measurement of aerosol composition from filters was very limited (Schmeling et al., 2000).

Thus, the identification of aerosol composition classes relied on other measurements that do not provide direct evidence of aerosol composition but correlate well with the presence of certain air mass types. The ancillary data utilized were particle size distributions (Collins et al., 2000), air mass backtrajectory (Verver et al., 2000), spectral dependence of the aerosol optical depth (Schmid et al., 2000) and dry scattering coefficients (Öström and Noone, 2000), altitude of the plane and visual recognition. In particular, the shape and particle concentration of the accumulation mode in the number size distribution was used to differentiate between aerosol from polluted and clean events. Those flight passes in which the air mass type, as indicated by back-trajectories, was coming from Europe, the size distribution showed high concen-

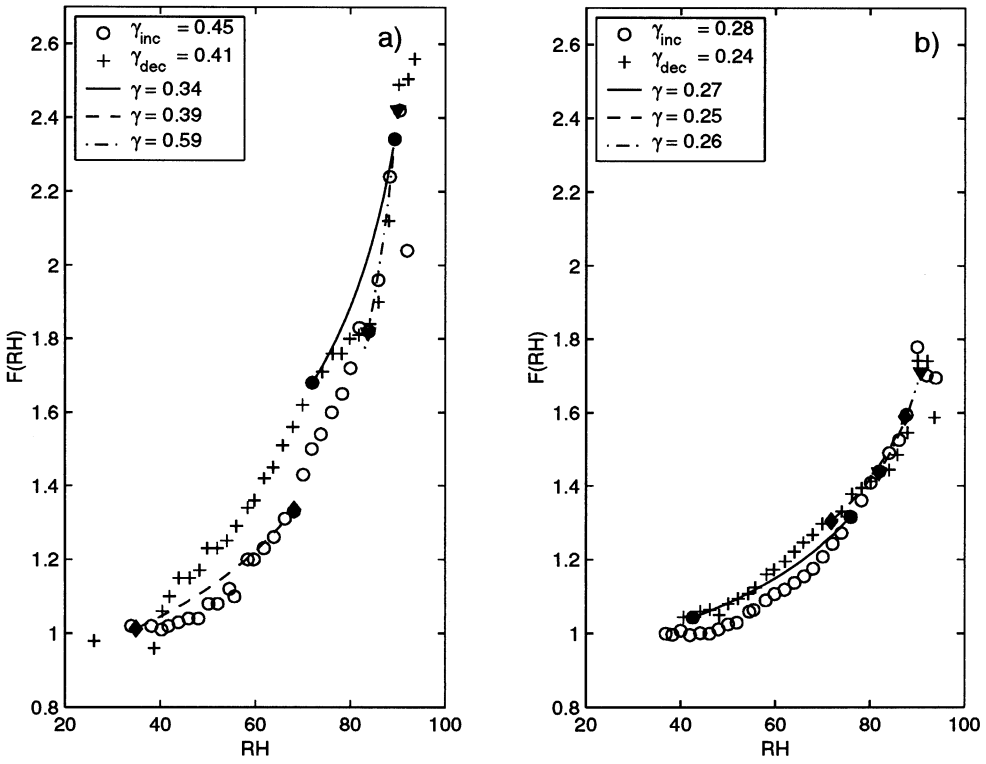

Fig. 2. Plot of $F(\mathrm{RH})$ $(=\sigma_{sp}(\mathrm{RH})/\sigma_{sp}(\mathrm{RH_o}))$ versus RH for a clean marine air sample taken during ACE-1 (panel a) and a polluted air sample taken in Sagres during ACE-2 (panel b). The ○ and + symbols correspond to the increasing and decreasing RH scans of the same aerosol sample respectively. Two point fits are shown for selected pair of points both above and below the deliquescence point (~82% in panel a) and RH = 75% (in panel b) as well an intermediate example.

trations of particles in a single accumulation mode, and the plane was flying in the lowest 600 m were labeled "polluted marine". The aerosol type "clean marine" was identified by size distributions with low concentrations, with 1 or 2 modes near the 0.06–0.3 μm diameter range and air mass coming from a region of clean air such as the central North Atlantic. Measurements of dust were easier to identify by the sharp increases in σ_{sp}, the low spectral dependence of aerosol optical depth and scattering coefficient and a noticeable coarse mode. The dust outbreaks were sampled always in the free troposphere (above $z = 2.20$ km) over the sea, and over Tenerife Island when flying near the lidar at the ACE-2 site at Izaña.

An example of actual scattering coefficients measured by UWPH is displayed in the left panel of Fig. 3. It corresponds to a CLEARCOLUMN profile of 8 July (flight 15), i.e., a profile where no clouds were present. Back-trajectory analysis indicates that the boundary layer air mass originated in the British Isles and passed through Spain, whereas the free troposphere originated in the mid-Atlantic west of the Canary Islands (Verver et al., 2000). In addition, based on AVHRR imagery (Durkee et al., 2000), the north edge of a Saharan dust plume reached the Canary Islands region. Filter measurements available for this flight in the layer aloft also indicated the presence of dust (Schmeling et al., 2000). The selection criteria discussed above thus suggest that 3 aerosol types could be distinguished in the data measured by the UWPH. They correspond to dust (aloft), free tropospheric (middle layer) and marine polluted aerosol in the lower first km. The difference between σ_{wet} and σ_{dry} indicates the presence of a

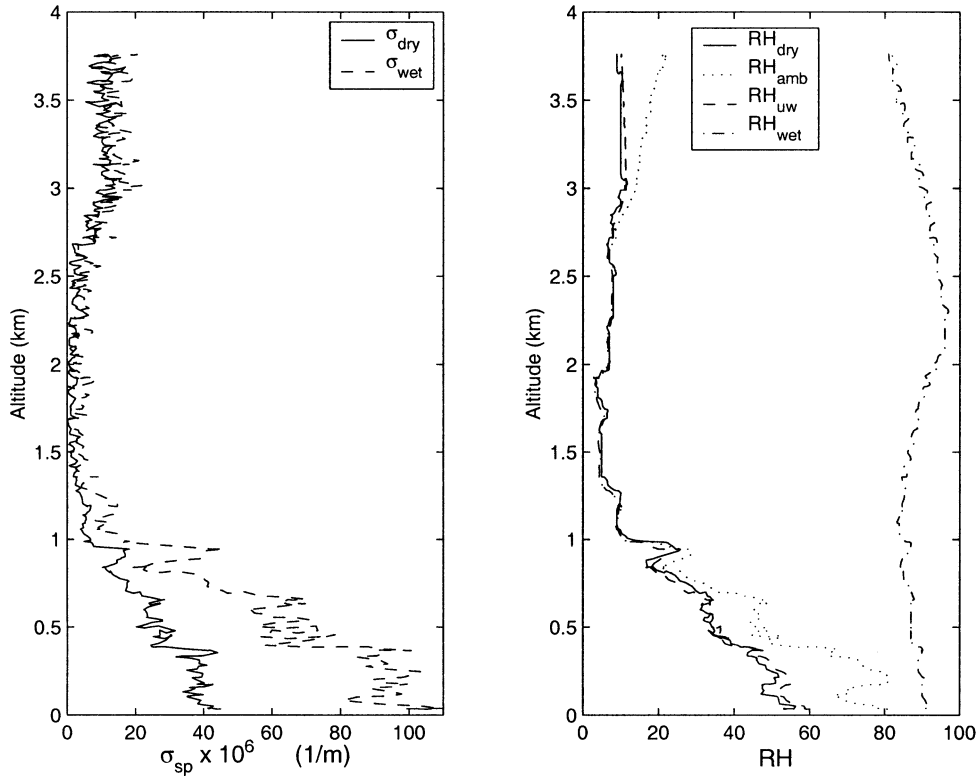

Fig. 3. Example of scattering coefficients and relative humidities measured by the UWPH on 8 July (flight 15). Left panel: scattering coefficient measured by the hydrated nephelometer (σ_{wet}) and dry nephelometer (σ_{dry}) as a function of height. Right panel: RH in the hydrated (RH_{wet}) and dry (RH_{dry}) nephelometers, ambient RH (RH_{amb}) and RH measured at the inlet of the UWPH (RH_{uw}). A 5-point running average has been applied to data in the right panel for purpose of clarity.

layer with high hygroscopicity near the surface and low hygroscopicity in the upper part of the profile, in accord with the classification scheme.

The procedure for the derivation of γ basically consisted in the selection of a flight interval of interest and then application of a quality assurance filter to the scattering coefficients measured by the UWPH. This procedure was adopted after finding out during the field campaign that high temperatures inside the plane dried the UWPH system significantly more than was projected. This effect is displayed in the right panel of Fig. 3 where 4 relative humidities are shown: RH_{wet}, RH_{dry}, RH_{amb} and RH_{uw}. The latter is the relative humidity measured at the tee before the dry and wet nephelometers (Fig. 1). In the bottom first kilometer where the ambient humidity is high, it is clear that the RH at the entrance of the UWPH (dashed line) is significantly lower than RH_{amb} (dotted line). Further, the relative humidity in the hydrated nephelometer (RH_{wet}) was above 80%. However, there were cases when RH_{wet} dropped below 60% in many instances, i.e., well below the deliquescence point of marine salt particles. Thus, in those aerosol samples that did effloresce (it is not clear how common this was), the "wet" nephelometer was not measuring aerosol in the hydrated state. The smooth curve of eq. (1), from which γ is derived, provides a reliable estimate only if the ambient aerosol is in its hydrated state. Thus, if the 2-point fit includes a measurement of an effloresced aerosol, the derived γ will be in error. In order to insure that the wet nephelometer measurements are on aerosols in a hydrated state, a threshold relative humidity (RH_{thr}) was used to discard the records (i.e., one record is one set of

measurements RH_{wet}, RH_{dry}, σ_{wet} and σ_{dry} taken every 6 s) with RH_{wet} below this limit. The Rood et al. (1989) study showed that hydrated aerosols (metastable droplets) decrease in frequency as RH drops but still exist more than 50% of the time when ambient RH is between 45% and 75% (in the 3 continental sites studied). Since a similar statistical study on marine particles is not available, we assume that the same proportion is applicable to the particle measurements of the UWPH. The specific value of RH_{thr} was set to 60% and is discussed further in the next section where the sensitivity of the derived γ to RH_{thr} is studied.

In summary, the procedure for deriving γ was as follow: (i) select a flight interval of interest (referred to as a "pass"), e.g., a constant altitude segment or where $RH_{amb} \sim$ constant or $\sigma_{sp} \sim$ constant; (ii) determine the aerosol composition type (dust, marine clean or polluted); (iii) discard records which do not fulfill $RH_{wet} > RH_{thr}$; (iv) least square fit of eq. (1) to the remaining records.

In some flights, it was possible to include the data of the MISU nephelometer (Öström and Noone, 2000), to the fitting of eq. (1). However, no changes were observed in the average value of γ when this third RH point was utilized. Also, there are few good data points for clean free tropospheric air since in these cases σ_{dry} was near the noise level of the dry nephelometer and the ambient RH was so low that RH_{wet} was rarely above 50%.

It is important to note that the relatively low size cut-off of the inlet probe was a problem with regard to the sampling of salt particles or dust since a significant number of such particles were above the 2.5 μm size cut of the inlet (note the low scattering coefficients in the dust layer in Fig. 3 are due partially to this effect; see also Collins et al. (2000) for more effects of the cut-off). Although it did not represent a problem in determining γ, this size restriction limited the applicability of the UWPH derived data set to particles up to 2.50 μm in diameter. Finally, the airflow through the nephelometers at the reduced pressure of higher altitudes was slower than expected, resulting in an unacceptably slow time response. To correct for this, a first order differential transform was applied to the raw data: $\sigma_{sc}^{corr}(t_i) = \sigma_{sc}^{measured}(t_i) + \Delta\sigma_{sc}/\Delta t \cdot \tau$, where τ is the sampling volume of the nephelometer divided by the flow rate.

4. Analysis of aerosol hygroscopicity

4.1. *Impact of hysteresis and RH_{thr} on the derived γ's*

As was mentioned in Subsection 3.2, frequently RH_{wet} was below 80%, either because of drying inside the plane or because RH_{amb} was too low. For aerosols with a high deliquescence point, this may result in an underestimation of γ. For example, this effect could be significant when studying clean marine samples since some laboratory studies suggest they will effloresce (Tang and Mulkewitz, 1994; Cziczo et al., 1997). Thus, we have adopted a selection criteria based on a threshold value of RH_{wet} sufficiently high to avoid this problem. In this section, we study the sensitivity of γ to the threshold value.

The exponent γ was derived for a selection of threshold values, namely $RH_{thr} = 60$, 70, 80 and 85%. The derived γ's are displayed in the histograms of Fig. 4. The top row (4a–c) shows histograms of γ for different threshold in the clean marine aerosol passes. Each data point in the histogram represents the γ obtained after averaging all records throughout a pass. The average and standard deviation of γ over all passes is included in each histogram. The effect of drying due to aircraft heating reduces the number of records with high RH_{wet}. In fact, there are no records when $RH_{thr} = 85\%$. Figs. 4a,b do not show a significant change in the average γ with RH_{thr}. Fig. 4c shows γ's which are indicative of a growth curve with a deliquescence point between 70% and 80%. However, it is representative of only 5 passes from 1 flight (flight 05, 23 June). A similar analysis was performed on marine polluted samples. In this case, no significant change was observed in γ as a function of RH_{thr} and no clear trend suggestive of hysteresis can be discerned (Figs. 4d–g). While this filtering with a high RH_{thr} reduced significantly the number of records in a given pass (to less than 6% of the samples on some occasions), the sensitivity of the retrieved γ to RH_{thr} was not great, suggesting that the aerosol did not effloresce until relatively low RHs were achieved. In fact, in the majority of the passes, most of the data points remained after the filtering.

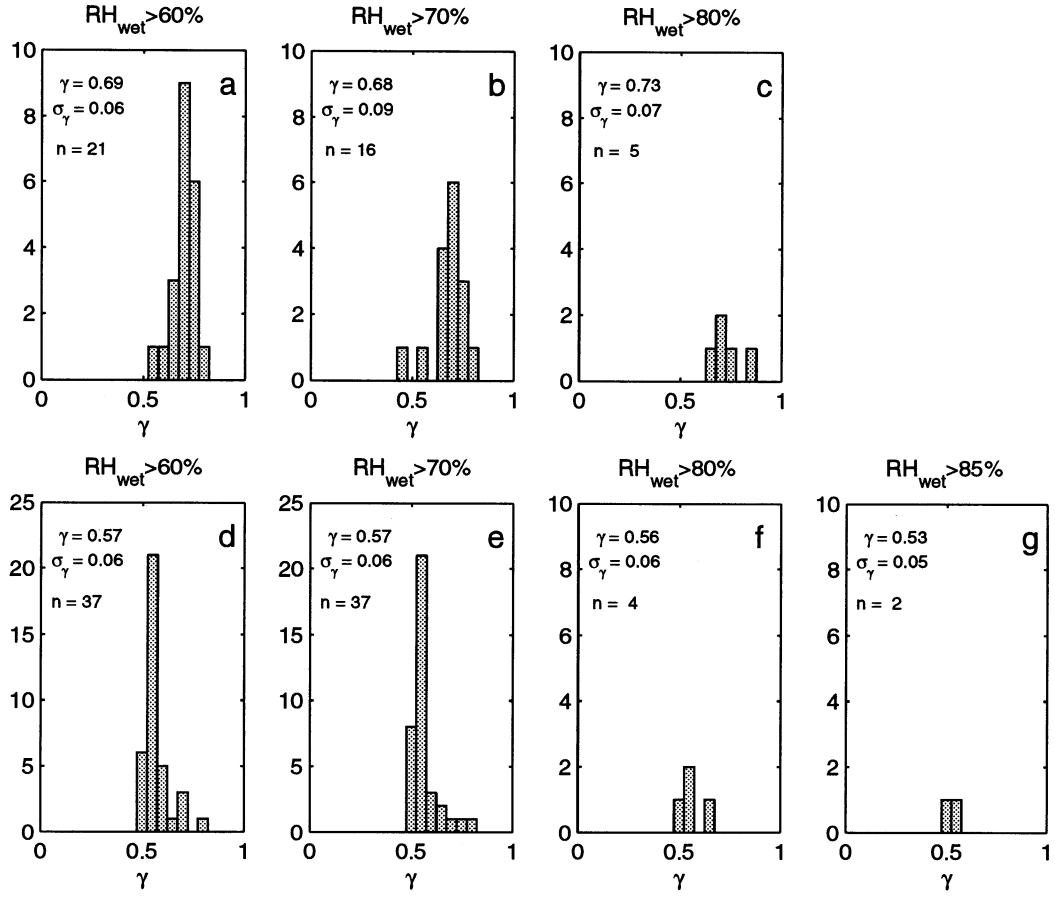

Fig. 4. Histograms of γ for clean marine (top row, 4a–c) and polluted marine aerosol (bottom row 4d–g) for different conditions on RH_{wet}. γ = mean, σ_γ = standard deviation, n = number of flight segments used in obtaining mean γ.

For example, on average in the clean marine cases, nearly 100% of the points of a pass remained after using the 60% RH_{thr} criteria. On the other hand, in the presence of particles that deliquescence, the specific value of RH_{thr} may have an effect on γ, as illustrated in Figs. 4b,c. However, the differences noted here are not statistically significant.

This analysis also shows that the selection of RH_{thr} in the range 60–70% is not critical in the derivation of γ for the polluted marine samples observed in this study (Figs. 4d,e).

These results are in accord with other studies conducted in ACE-2. Oftentimes, the Pelican sampled aerosols advected 24–48 h after their passage through the ACE-2 ground station at Sagres, Portugal (Carrico et al., 2000). While not sampling the same aerosol as the Pelican, at least concurrently, some useful general comparisons can be made. Clean air humidigraphs of $\sigma_{sp}(RH)$ at this station showed little or no deliquescence. During polluted conditions, humidigraphs at Sagres were also consistent with the Pelican measurements in showing no deliquescence. Similar observations have been noted at other ACE-2 sites that measured the variation of particle diameter as function of RH. For example, deliquescence was occasionally observed at the ground station of Punta del Hidalgo on Tenerife Island but it was not observed either at Sagres or on the R/V *Vodyanitsky* (Swietlicki et al., 2000).

In summary, this examination suggests that our method derives a realistic value of γ in a wide

range of relative humidities for the aerosol sampled in ACE-2. On the other hand, the method will likely fail to accurately derive σ_{amb} and could over or underestimate γ by as much as 100% in aerosol samples that do not follow eq. (1) (such as those in clean marine environments where marked deliquescence takes place).

4.2. Stratification by γ of aerosol type

The histogram in Fig. 5 summarizes the distribution of γs ($RH_{thr} = 60\%$) for the whole data set. The average γ for each of the 3 aerosol types used in this study, and the derived ratio $F(80\%) = \sigma_{sp}(RH = 80\%) / \sigma_{sp}(RH = 30\%)$ are shown in Table 1. The number of passes used in averaging γ is included. Each pass corresponds to a period of time when the airplane sampled the same aerosol parcel according to the criteria defined in Subsection 3.2.

The 3 aerosol types can be distinguished by their means. The distribution for polluted aerosol and clean aerosol selected with $RH_{thr} = 60\%$ overlaps slightly (based on their respective standard deviations). However, with the clean aerosol selected with $RH_{thr} = 80\%$, the overlap disappears and both distributions are statistically differentiable.

Dust aerosols generally show a much lower γ compared to polluted and clean marine aerosol. However, during this study there were observed cases of dust over Tenerife in which the γ exponent

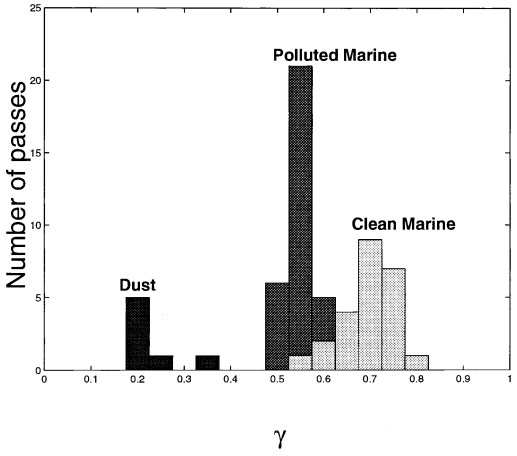

Fig. 5. Histogram of γ for the 3 different aerosol types.

Table 1. *Average γ, standard deviation (σ_γ), calculated ratio $F(80\%)$ $(= \sigma_{sp}(80\%)/\sigma_{sp}(30\%) = (0.7/0.2)^\gamma)$, error in $F(80\%)$ and number flight intervals of the same aerosol type from which a γ was computed (passes)*

Aerosol type	γ	σ_γ	F (80%)	ΔF (80%)	Passes
dust	0.23	0.05	1.33	0.07	7
polluted marine	0.57	0.06	2.04	0.16	37
clean marine 1	0.69	0.06	2.37	0.19	21
clean marine 2	0.73	0.07	2.50	0.23	5

Clean marine 1: clean aerosol samples with $RH_{wet} > 60\%$. Clean marine 2: samples with $RH_{wet} > 80\%$. See criteria for aerosol types in Subsections 3.2 and 4.2.

was significantly higher ($\gamma \sim 0.4$) than that of the dust measured over the ocean. Such a case was observed, for example when flying in the dust cloud over Tenerife island on 20 July (flight 20). A similar behavior was observed in dust mixed with free tropospheric air on 8 July (flight 15) and 20 July when the plane flew the between boundary layer and dust layer aloft. Since the compositional data available on the Pelican did not have spatial resolution comparable to the UWPH, these cases were difficult to classify and they are not included in the mean values in Table 1. These observations suggest that occasionally the higher hygroscopicity observed in dust may have been caused by mixing with aerosols from other origins (local sources in Tenerife or free tropospheric aerosols in the cases here mentioned). Ground measurements of dust hygroscopic factors (Li-Jones et al., 1998) suggest a similar behavior in dust samples taken at Barbados (13.17°N, 59.43°W). Li-Jones et al. observed that an important portion of the observed hygroscopicity of this dust is due to other aerosols externally mixed with the dust. In fact, Putaud et al. (2000) found important concentrations of hydrophilic species such as SO_4^{2-} and $CaCO_3$ in dust samples measured at the Izaña site (located at an altitude of 2.3 km) on Tenerife.

An example of the variability of γ in the boundary layer column is displayed in Fig. 6, where plots of γ, derived σ_{amb} and RH_{amb} versus altitude are shown for the profile of 8 July. The data displayed are 60 s averages and the error bars for σ_{amb} were computed as $\Delta\sigma_{amb} =$

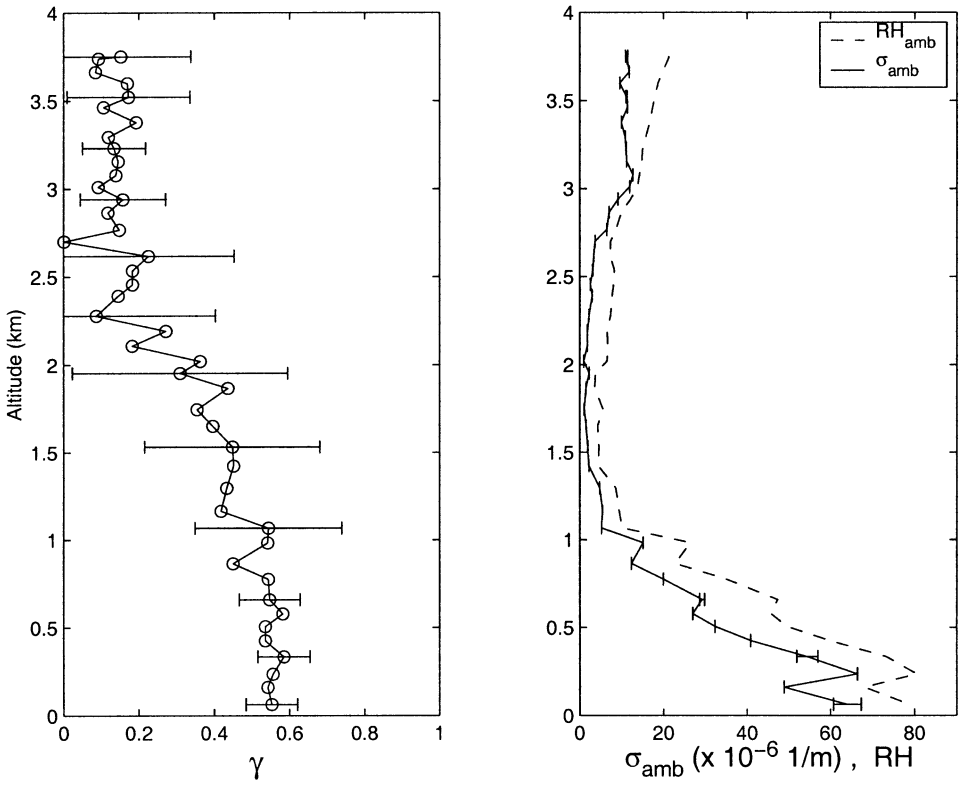

Fig. 6. Descending profile of γ (left panel), derived ambient σ_{sp} ($\times 10^{-6}$ l/m) and ambient RH (right panel) during the CLEARCOLUMN flight 15 (8 July).

$\sigma_{amb}(RH_{amb}, \gamma) - \sigma_{amb}(RH_{amb}, \gamma \pm \Delta\gamma)$. This case illustrates the 2 aerosol types that have been shown to be statistically differentiable for the whole data set (dust and marine polluted) and an example of γ in clear air in the free troposphere (1.0–2.7 km). This clean air pass in the free troposphere is one of only 2 flight segments observed in the entire data set where a γ for this aerosol type could be derived. More typically, when the plane sampled clean tropospheric aerosol it was characterized by low σ_{sp} and low RH_{amb} rendering a statistical analysis infeasible. In Fig. 6, the large uncertainty bars for the clean air reflect the effect of low scattering (near noise level). The large uncertainty in γ in dust is not reflected in the derived σ_{amb} because its uncertainty is modulated by the magnitude of RH_{amb} and the amount of drying when the aerosol gets into the UWPH.

Qualitatively, the γ's shown in Fig. 5 and in Table 1 are in agreement with previous studies. Although our classification of aerosol type did not rely on aerosol composition measurements, our indirect classification scheme distinguished 3 hygroscopic regimes. In the case of polluted and clean marine aerosols, our observations show that polluted samples have lower γ, that is, lower hygroscopic growth, than clean marine aerosols. This is consistent with numerous experimental studies (Kotchenruther et al., 1999; Saxena et al., 1995; Zhang et al., 1993) which show that aerosols with anthropogenic organic compounds tend to make the aerosol more hydrophobic. Also, our observations are in qualitative agreement with other sites that measured hygroscopic properties of aerosol in the ACE-2 region. For example, Carrico et al. (2000) observed at the site in Sagres, Portugal that aerosols sampled during European pollution outbreaks are less hygroscopic than clean air samples. Similar observations have been reported at Punta del Hidalgo, Tenerife Island and

on a research vessel taking samples in the Portugal–Canary Islands corridor (Swietlicki et al., 2000). The dust samples show lower, but not negligible, hygroscopicity compared to the other 2 types of aerosol. This observation agrees with Li-Jones et al. (1998) who found that ambient aerosol samples with a high content of dust have a hygroscopicity distinguishable from the other aerosols.

While a quantitative comparison of derived parameters with previously published data is not a straightforward task (few studies of σ_{sc} versus RH throughout a column of air over the ocean are available in the literature (Kotchenruther et al., 1999; Hegg et al., 1996) and fewer still have concurrent chemical composition data), our estimation of γ and the derived ratio $F(80\%)$ $(=\sigma_{sp}(80\%)/\sigma_{sp}(30\%))$ compare reasonably well with values for similar types of aerosols. For example, Hegg et al. (1996) obtained a clean marine $F(80\%)$ of 2.3 ± 0.3 (measured over the NE Pacific Ocean coast) and a mildly polluted/continental $F(80\%)$ of 1.7 ± 0.1. Similar agreement is found with the studies of Covert et al. (1972) (ground measurements in Denver and Seattle) and Fitzgerald et al. (1982) (ground measurements in the Washington, DC area). Li-Jones et al. (1998) report measurements of dust mixed with marine aerosols with an $F(80\%)$ ratio in the range 1.1–1.3 and, for pure dust, a range of 1.0–1.1.

On the other hand, Kotchenruther et al. (1999) reported higher values of $F(80\%) = 2.3 \pm 0.24$, in anthropogenic aerosols over the East Coast of the USA. With respect to other work in ACE-2, our measurements of polluted and clean marine aerosols have significantly larger γ's than those derived from the humidigraph measurements made at Sagres by Carrico et al. (2000). This disagreement is probably due to the fact that the Sagres site was exposed to continental aerosol sources and it is possible that the clean marine samples had some continental influence. This is suggested by the Swietlicki et al. (2000) study which found lower hygroscopicity for polluted and clean aerosol at the Sagres site compared to the sites on Tenerife Island and on the R/V *Vodyanistky*.

5. Simulation of the dependence of the upwelling radiance on aerosol hygroscopicity

Aerosol optical depths have been retrieved globally and routinely from AVHRR data available from currently operational NOAA polar orbiters (Durkee et al., 1991; Nagaraja Rao et al., 1989; Stowe et al., 1997). Also, aerosol optical depths and other aerosol parameters will be routinely retrieved by the MODIS and MISR detectors on board of the EOS-AM ("Terra") platform (King et al., 1992). The retrieval algorithms are based on a look-up table methods and they do not include aerosol hygroscopicity as one of the parameters to be retrieved (Tanré et al., 1997; Kahn et al., 1997). Given that these new detectors have better precision and more spectral bands, it is of interest to investigate if, for a pixel with known optical depth, there are any features in the upwelling radiance that can be related to an aerosol model with specific hygroscopic properties. In this section, we perform forward radiative transfer simulations with aerosol models of known optical and hygroscopic properties derived from the ACE-2 data set. The objective is to observe the effect on the upwelling radiance of aerosol models with different γ's. These simulations will help to assess whether a variation in aerosol hygroscopicity results in a distinctive change in radiance. It is not our intention in this exploratory study to perform an actual retrieval but rather to perform a preliminary assessment of the feasibility of performing such a retrieval.

5.1. *Model and detector features*

The simulated upwelling reflectances (radiances normalized to the solar constant and cosine of the Sun's zenith angle) were computed with the 6S code (Second Simulation of the Satellite Signal in the Solar Spectrum) (Vermote et al., 1997). 6S is a radiative transfer code specially designed for the simulation of radiances measured by satellite detectors in ultraviolet, visible and near infrared wavelengths (0.25–4.0 μm). The code uses measured data or standard models of atmospheric profiles of temperature, water vapor and other gases. The aerosol size distribution can defined by the user or the user can choose one of the many built-in models frequently employed in the literature (D'Almeida et al., 1991; WCP, 1986). In addition, the ground reflectance is simulated by the option of several land and ocean (lambertian and non-lambertian) models. The gaseous atmospheric transmission is determined by using random exponential models with a 2.5 nm spectral

resolution. One of the limitations of the code is that only one size distribution (internally mixed) can be used in each run. Also, the vertical aerosol concentration is fixed by the code with an exponential function with scale height of 2 km. As is customary in many radiative transfer codes, the optical depth ($\lambda = 550$ nm in this case) at the surface is set by the user and the corresponding radiance is computed. The aerosol scattering phase function, single scattering albedo, and scattering coefficient are computed internally by a Mie code. Then, the code uses a successive order of scattering method to determine the scattering properties of the Rayleigh-aerosol system. For more information, the reader is referred to the user manual (ftp://kratmos.gsfc.nasa.gov/6S/).

The radiance was computed at the wavelength bands suitable for aerosol retrievals by the EOS-AM, MODIS and MISR spectrometers. The MOderate Resolution Imaging Spectroradiometer (MODIS) detector is a multispectral (36 bands) imager designed to measure biological and physical processes such as concentration of chlorophyll, cloud properties, fire occurrence and size, and vegetative conditions (King et al., 1992). In particular, MODIS has 7 bands in the visible and near infrared (centered at 470, 555, 659, 865, 1240, 1640 and 2130 nm) potentially useful for the retrieval of aerosol size distribution parameters and optical depth (Tanré et al., 1997). MODIS is a downlooking sensor with a 2330-km wide ground swath and pixel resolution at nadir of 250 to 1000 m depending on the band. In contrast, MISR is a multiangle imaging system which acquires data with a 360-km swath at 9 angles spread out in the forward and after direction in 4 spectral bands (446, 558, 672 and 866 nm) (Diner et al., 1989). The forward and afterward cameras are paired in a symmetrical arrangement and set at fixed view angles on the optical bench. The nominal angles with respect to the earth's surface are 0, 26.1, 45.6, 60 and 70.5° (labeled Nadir, Af/Aa, Bf/Ba, Cf/Ca and Df/Da where the f and a suffixes refer to forward and after looking cameras, respectively). Data from these cameras will permit the derivation of aerosol optical depth, and aerosol type (which represents a combination of index of refraction, size distribution and particle shape) at a ground spatial resolution of 17.1 km (Kahn et al., 1997, 1998).

5.2. *Adjustment of the in-situ data*

In order to make the computer simulations, a number of adjustments to the measured data were applied. Two measured dry size distributions representative of typical aerosols found during ACE-2 were selected: marine clean (21 June, flight 03) and marine polluted (10 July, flight 17) (Collins et. al., 2000). The 2 distributions were obtained by averaging the measured distributions over the marine boundary layer profiles. Due to their low hygroscopicity, dust distributions were not considered in the simulations. Since a single size distribution and refractive index have to be specified in each run, a total of 8 size distributions were generated for different combinations of γ (= 0.2, 0.4, 0.6, 0.8) and RH_{amb} (= 30% and 85%) for each of the 2 aerosol types simulated. Then, the upwelling radiance of each distribution was computed. The modification of the radius and the refractive index of the size distribution as a function of RH and γ are explained as follows.

The dependency of the radius (r) on RH and γ was obtained by assuming a relationship between the volume of the particles and the scattering coefficient at the same RH:

$$\left(\frac{r(\mathrm{RH})}{r(\mathrm{RH_o})}\right)^3 \cong \frac{\sigma_{sp}(\mathrm{RH})}{\sigma_{sp}(\mathrm{RH_o})} = \left(\frac{1-\mathrm{RH_o}}{1-\mathrm{RH}}\right)^{\gamma}, \qquad (2)$$

where RH_o is a reference relative humidity. This relationship assumes that the Mie efficiency factor $Q_{scat}(\lambda, r, n) \sim kr$ (where k is a constant). This approximation is valid if most of the particles are within the size range 0.1–1.0 μm diameter where the Mie scattering efficiency is indeed approximately proportional to the particle radius. σ_{wet} and σ_{dry} (thus the derived γ's) obtained during ACE-2 are representative of particles up to 2.50 μm (aerodynamic diameter). However, due to the relative sampling efficiency of the system and the relative number of particles of various sizes below 1 μm compared to the number in the 1.0–2.5 μm size range, we can assume that most of the scattering measured (and the hygroscopic properties derived) is representative of particles in the $Q_{scat}(\lambda, r, n) \sim r$ optical range. Certainly, we would not expect significant differences in hygroscopicity between particles in the 0.1–1.0 μm size range and those between 1.0 and 2.5 μm, a difference necessary to undermine the applicability of our γ estimates. The extension of the measured γ

Table 2. *Size distribution parameters and optical properties at a reference index of refraction (n) and wavelength ($\lambda = 550$ nm). The size distributions cover the 0.01–6 μm diameter size range*

	V_{tot} ($\mu m^3/cm^3$)	N_{tot} (cm^{-3})	$R_{vol,acc}$ (μm)	$R_{vol,coa}$ (μm)	R_{eff} (μm)	n	w_o	$\langle\cos(\Theta)\rangle$	σ_{sp} (m^{-1})
polluted	18.1	1411	0.10	1.54	1.18	1.49, 1e-2	0.875	0.67	4.35e-5
clean	1.9	581	0.08	1.47	1.37	1.45, 3e-3	0.937	0.69	3.06e-6

V_{tot} = total volume of the distribution, N_{tot} = total number of particles in the distribution, $R_{vol,acc}$ = mean volume geometric radius in the 0.01–1 μm range, $R_{vol,coa}$ = mean volume geometric radius in the 1–6 μm range, R_{eff} = effective radius, n = real and imaginary part of the dry index of refraction, w_o = single scattering albedo, $\langle\cos(\Theta)\rangle$ = asymmetry factor, σ_{sp} = scattering coefficient.

to particle sizes beyond 2.50 μm depends on the compositional partition of the aerosols as a function of size. In size distributions with low contrast in composition (more specifically, hygroscopicity) between the coarse and accumulation modes, like marine polluted or clean marine, this assumption may be valid; in cases when a dust coarse mode is present, this assumption is not true.

The input aerosol model in 6S requires an internally mixed aerosol size distribution. The index of refraction used in each run was obtained by volume weighting according to Hanel's formula (1976):

$$n_{r,i}(\mathrm{RH}) = n_{r,i}(\mathrm{water}) + [n_{r,i}(\mathrm{dry}) - n_{r,i}(\mathrm{water})] \times \left[\frac{V(\mathrm{dry})}{V(\mathrm{RH})}\right], \quad (3)$$

where $n_{r,i}$ are the real and imaginary part of the index of refraction, V(dry) and $n_{r,i}$(dry) are the volume and refractive index of the particle in a dry state and V(RH) is the volume of the particle at ambient relative humidity. The dry index of refraction for both aerosol distributions is based on the chemical apportionment of clean and polluted measurements made at the Hidalgo station on Tenerife Island (measurements labeled MBL background and MBL Europe in Putaud et al. (2000)). For each dry distribution, the index of refraction of each component was weighted according to the chemical apportionment. The index of refraction of each component was obtained from Lenoble (1993) and Krekov (1992). In the Putaud et al. (2000) study, the proportion of soot found in the clean samples exceeded that of the polluted samples resulting in a higher single scattering albedo (ssa) in the polluted aerosol than the clean. However, in situ measurements of ssa on the Pelican (Öström and Noone, 2000) show that the clean aerosol samples have a ssa higher than the polluted aerosols. For consistency, the proportion of soot in the partition of aerosol composition was modified in order to produce a polluted ssa smaller than the clean one.

Figs. 7a,b display the dry size distributions used in the computer simulations. Table 2 lists the main features of each along with some optical properties (used in the model) computed at a reference index of refraction and wavelength. Both distributions exhibit a coarse mode but the particle concentration in the polluted distribution is considerably higher than the marine. This large difference in particle concentrations is significant in the optically active range 0.1–1.0 μm and it is reflected in the magnitude of the respective σ_{sp}s. The effective radius (R_{eff}) is a parameter frequently used in remote sensing computations and is defined as the ratio between the third and second moment of the particle size distribution (Hansen and Travis, 1974). The asymmetry factor ($\langle\cos(\Theta)\rangle$) is the average cosine of the scattering angle weighted by the size distribution's phase function. It is equal to 1 if all the incident energy is scattered in the forward direction and equal to -1 if all energy is back-scattered.

The reflectance generated by each distribution with a columnar load corresponding to $\tau_{aer}(550\ \mathrm{nm}) = 0.05, 0.15, 0.3$ and 0.7 was simulated in each camera of MODIS and MISR. One viewing geometry was modeled in which MISR and MODIS would observe the same pixel in the same pass: solar zenith angle of 55°, satellite (zenith) viewing angle of 5° and the difference between the Sun and satellite azimuthal angles of 90°. Sixty-four reflectances were generated for each camera

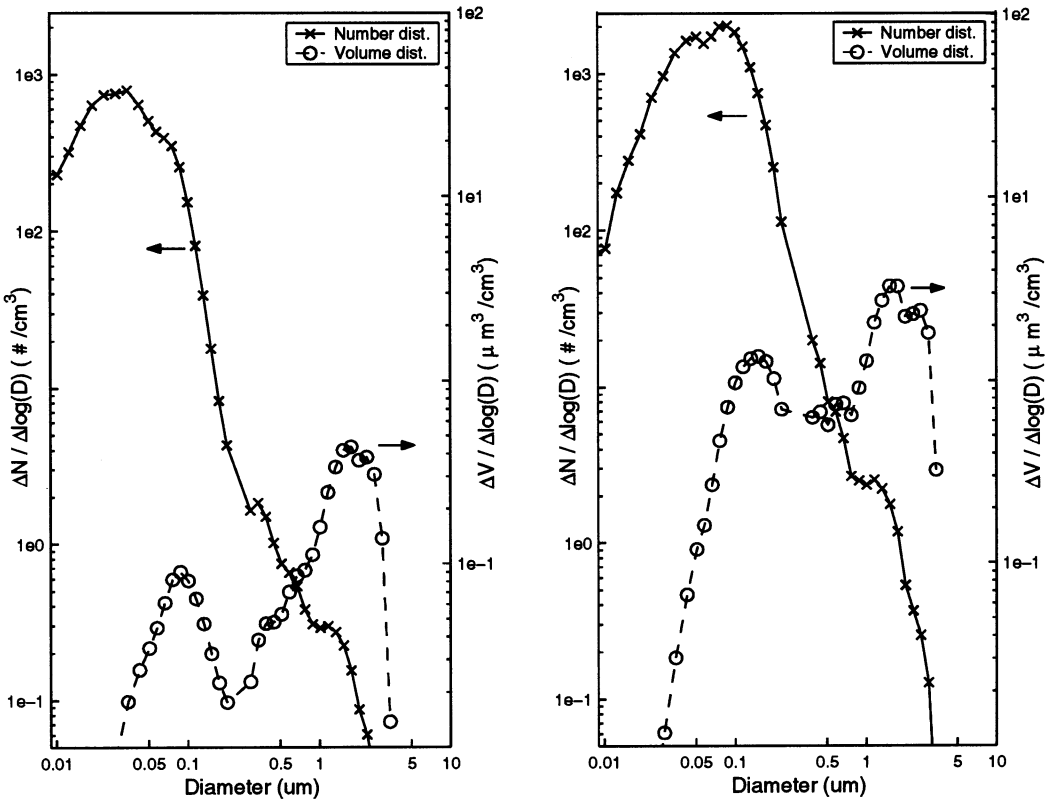

Fig. 7. Clean (left panel) and polluted (right panel) aerosol size distributions averaged over the marine boundary layer.

and each band corresponding to 2 dry size distributions (clean and polluted) with 2 RH_{amb}, 4 γ and 4 aerosol optical depths.

5.3. *Model results and discussion*

Fig. 8 displays the spectral reflectance of aerosols (ρ_{atmos}) only (i.e., excluding the contribution of the ground and the environment in the satellite signal) for the polluted and clean conditions in the 7 bands of MODIS. The spectral reflectance shows little dependence on changes in aerosol composition (γ) at low and moderate optical depths. At larger optical depths, it appears that a differentiation in composition (i.e., size distributions with different γ and the same RH_{amb}) is observed in the near infrared bands (above 865 nm) but, overall, no distinctive signal is observed for variations in ambient humidity. This behavior is not surprising considering that in each run, τ(550 nm) is held constant and the model adjusts the vertical aerosol concentration to compensate for the increase of scattering due to water take-up. It is important to note that there is not such constraint at infrared wavelengths.

A similar behavior is observed in the nadir camera of MISR. In the example shown in Fig. 9, which corresponds to a polluted aerosol with a moderate optical depth, the slope of the spectral dependence agrees with the first 4 bands of MODIS. The forward and after cameras show little dependence of the angular distribution of scattering on humidity effects. When the aerosol load increases ($\tau_{aer} = 0.7$, Fig. 10), a distinctive differentiation between reflectances corresponding to aerosols with the same γ but different RH_{amb} is observed in the forward cameras Df and Cf (forward looking cameras at 70.5 and 60.0° from the nadir of the satellite). A similar behavior is observed in the clean marine cases (not shown).

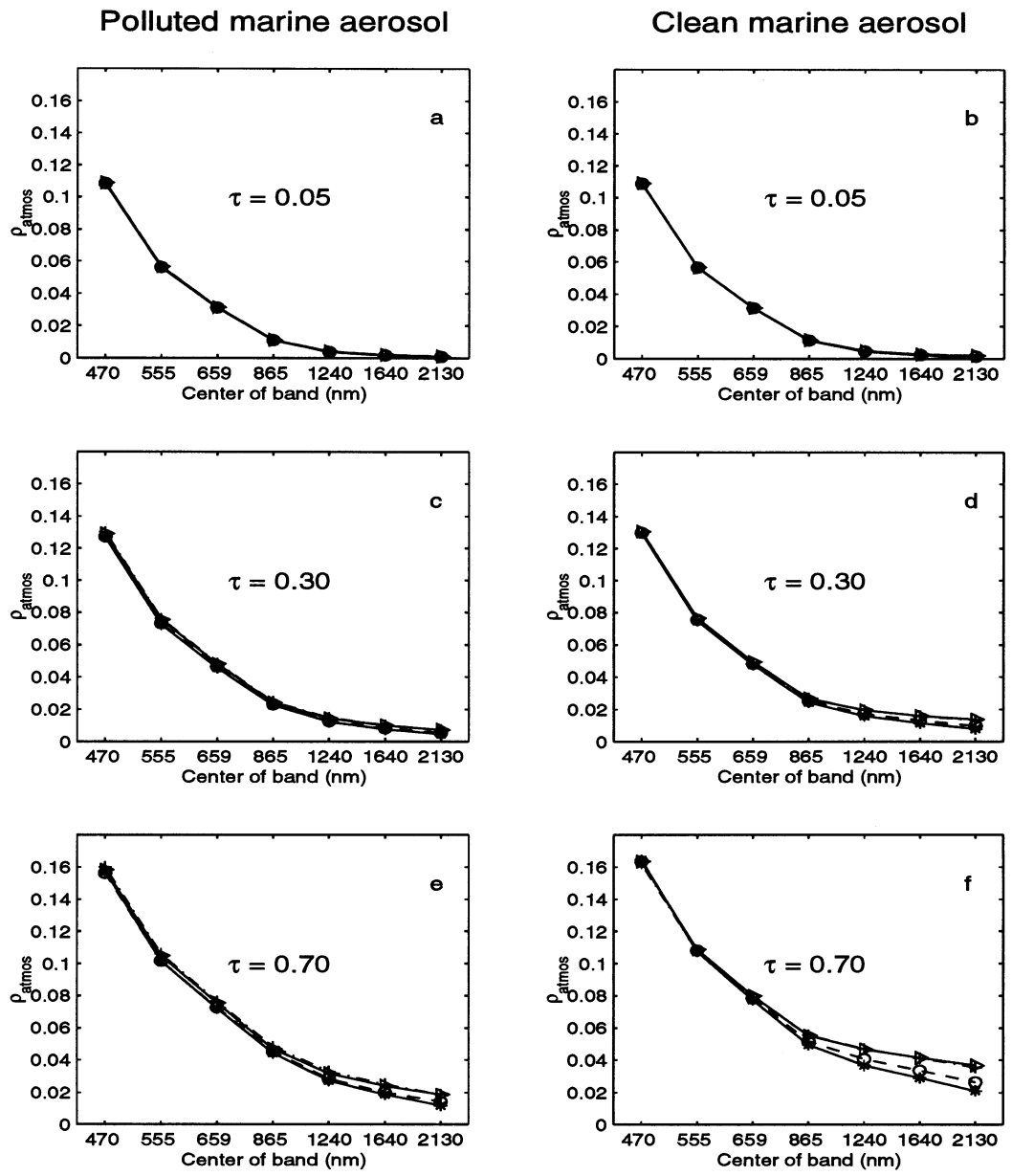

Fig. 8. Spectral dependence in MODIS bands (center of bands in nm) of the atmospheric reflectance (ρ_{atmos}) for the pollution (panels a, c, e) and clean (panels b, d, f) marine aerosol models at aerosol optical depths $\tau(\lambda = 550\ \text{nm}) = 0.05$, 0.30 and 0.70. Symbols: solid line with triangles: $\gamma = 0.4$ and $RH_{amb} = 30\%$, dashed line with circles: $\gamma = 0.8$ and $RH_{amb} = 30\%$, dash-dotted line with pluses: $\gamma = 0.4$ and $RH_{amb} = 85\%$, solid line with asterisks: $\gamma = 0.8$ and $RH_{amb} = 85\%$.

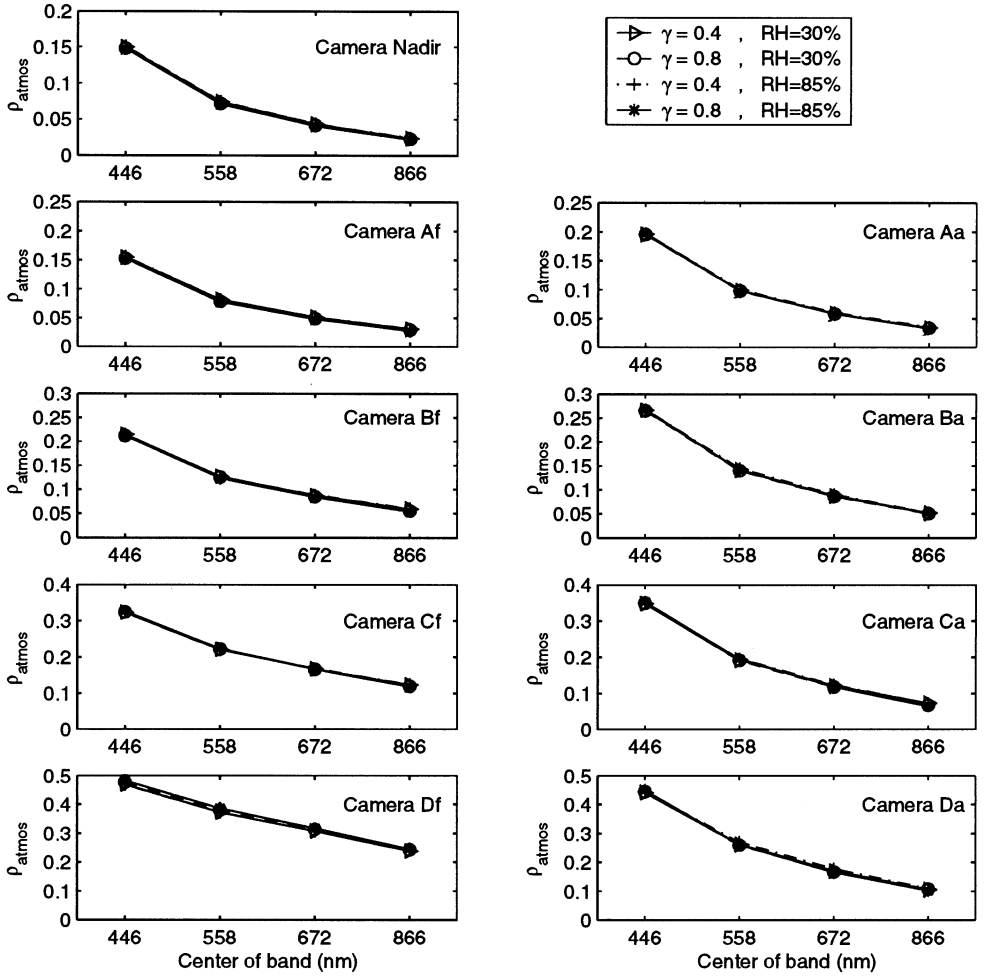

Fig. 9. Spectral dependence of the atmospheric reflectance (ρ_{atmos}) in the 9 cameras of MISR at the center of the bands (in nm) for the polluted marine aerosol model with an optical depth of 0.30 (at 550 nm). Nadir viewing camera is in the top row, forward looking cameras are in the left column (labeled Af, Bf, Cf and Df, see text for viewing angles) whereas the after looking cameras are in the right column. Symbols: same as in Fig. 8.

In summary, it is clear in Figs. 8–10 that relative humidity effects on particle size have little spectral "signature" in the visible range when comparing radiance from typical aerosol models until unusually high optical depths and viewing conditions (in the case of MISR) are considered.

However, it appears that aerosol distributions with different γ's may have distinctive reflectances at moderate optical depths in the NIR bands of MODIS, and MISR at the large angles. In Fig. 11, atmospheric reflectance versus RH_{amb} is plotted for band 7 (2100 nm) of MODIS. In Fig. 12, the same parameters are plotted for band 4 (860 nm, cameras Df, Cf and Da) of MISR. For each aerosol type considered, the reflectances generated by distributions with 3 different γ's (0.4, 0.6, 0.8) at several ambient humidities (= 30, 45, 60 and 80%) are displayed. The error bars correspond to the MISR and MODIS required preflight calibration uncertainties in the detectors (6% in MISR and 2% in MODIS, Butler et al., 1998). Fig. 12 shows that, although the reflectance varies as a function of the ambient humidity, this variability will possibly not be high enough to be resolved by the

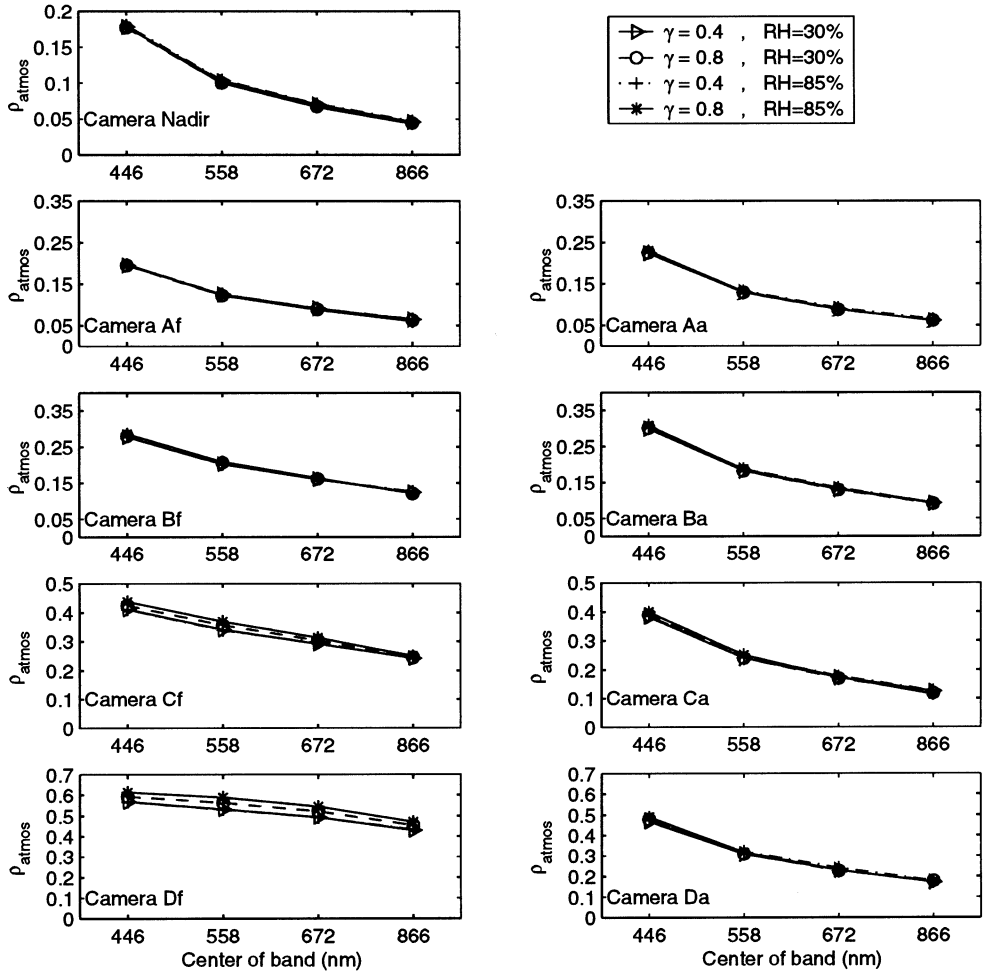

Fig. 10. Spectral dependence of the atmospheric reflectance (ρ_{atmos}) in the 9 cameras of MISR at the center of the bands (in nm) for the polluted marine aerosol model with an optical depth of 0.70 (at 550 nm). Nadir viewing camera is in the top row, forward looking cameras are in the left column (labeled Af, Bf, Cf and Df, see text for viewing angles) whereas the after looking cameras are in the right column. Symbols: same as in Fig. 8.

detection limit of MISR. However, in the near-infrared bands, particularly the 2100 nm band, MODIS seems to be able to resolve reflectances from aerosol distributions with different hygroscopic factors, that is, the detector's uncertainty associated with each reflectance is small compared to the difference in reflectances at a fixed RH. Fig. 11 indicates that for an aerosol scenario with a given optical depth, ambient RH and known aerosol type (polluted or clean), the aerosol models with different γ (i.e., different hygroscopic behavior) have distinguishable reflectances. The differentiation is apparent in models with different γ's and with the same γ's at different ambient RH as well. This effect is observed at low and high optical depths in the 2 aerosol size distribution types used in these simulations. Fig. 11 also shows that the difference between reflectance for polluted and clean conditions at similar optical depths is comparable to the differences due to variations of RH in the same model. This indicates that in order to detect a "γ signal" relative to an RH effect on the aerosol, a knowledge of the aerosol type must be known beforehand.

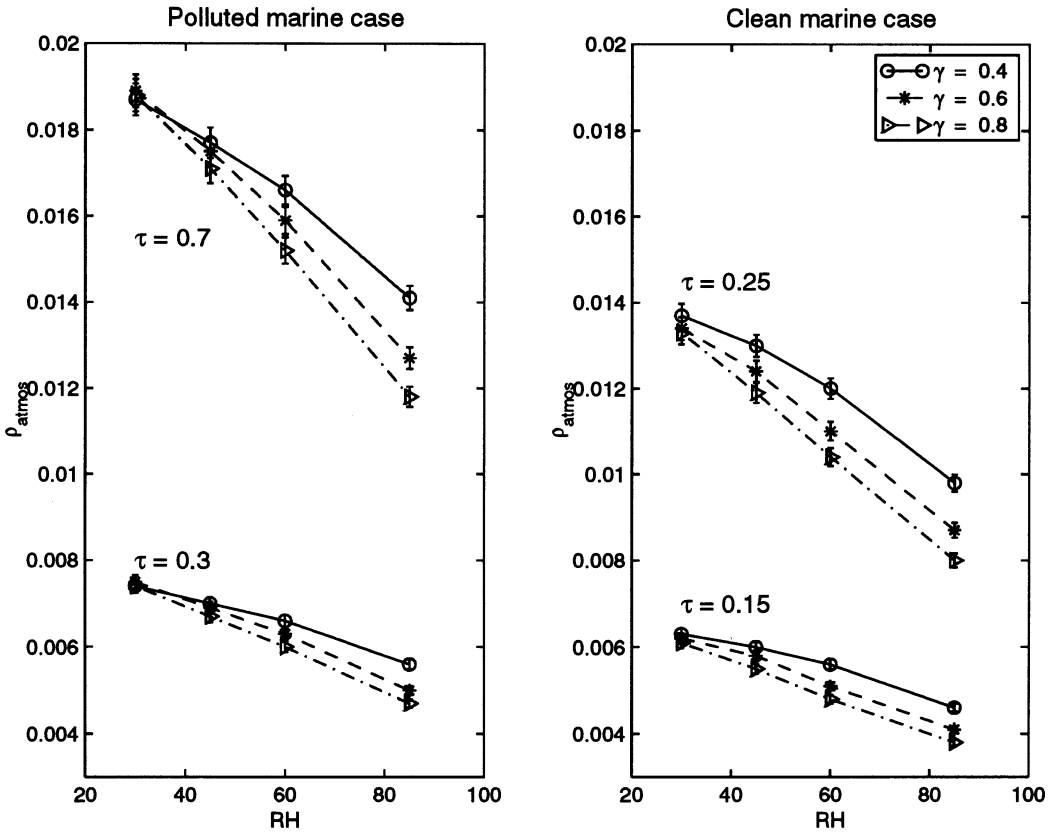

Fig. 11. Atmospheric reflectance (ρ_{atmos}) as a function of the ambient relative humidity for the polluted (left panel) and clean marine (right panel) aerosol in the 2100 nm band of MODIS. The top group of lines correspond to models with fixed $\tau(\lambda = 550\text{ nm}) = 0.70$ and the bottom 3 correspond to $\tau(\lambda = 550\text{ nm}) = 0.30$. The solid line correspond to a model with $\gamma = 0.4$, dashed line to $\gamma = 0.6$ and dash-dotted to $\gamma = 0.8$. The error bars are the nominal calibration uncertainties associated to the band.

6. Conclusions

In this paper, we have presented a methodology based on measuring the scattering coefficient at known humidities below and above ambient conditions, to derive airborne ambient scattering coefficients and aerosol hygroscopic properties with high time and spatial resolution. We implemented this methodology to obtain the aerosol ambient light-scattering coefficient and a measure of the aerosol hygroscopicity, the exponent γ, during ACE-2.

Although we did not have actual measurements of ambient scattering coefficients to compare with during the experiment, we believe that if the above and below ambient measurements are made at relative humidities not too far apart from each other, the method is robust enough to generally derive σ_{amb}. Concurrently, we have derived the exponent γ for a tripartite stratification of aerosols typical of the Canary Islands region (clean and polluted marine aerosols and dust).

In the second part of this paper, we studied the feasibility of finding a distinctive "signature" of ambient humidity effects on aerosol in spectral reflectances measured by satellites. We simulated a satellite signal with the help of the radiative code 6S and used data from ACE-2 (such as aerosol size distributions and hygroscopic parameters) as inputs to the model. This preliminary study suggests that the spectral signature in the visible bands of MISR and MODIS is not distinct-

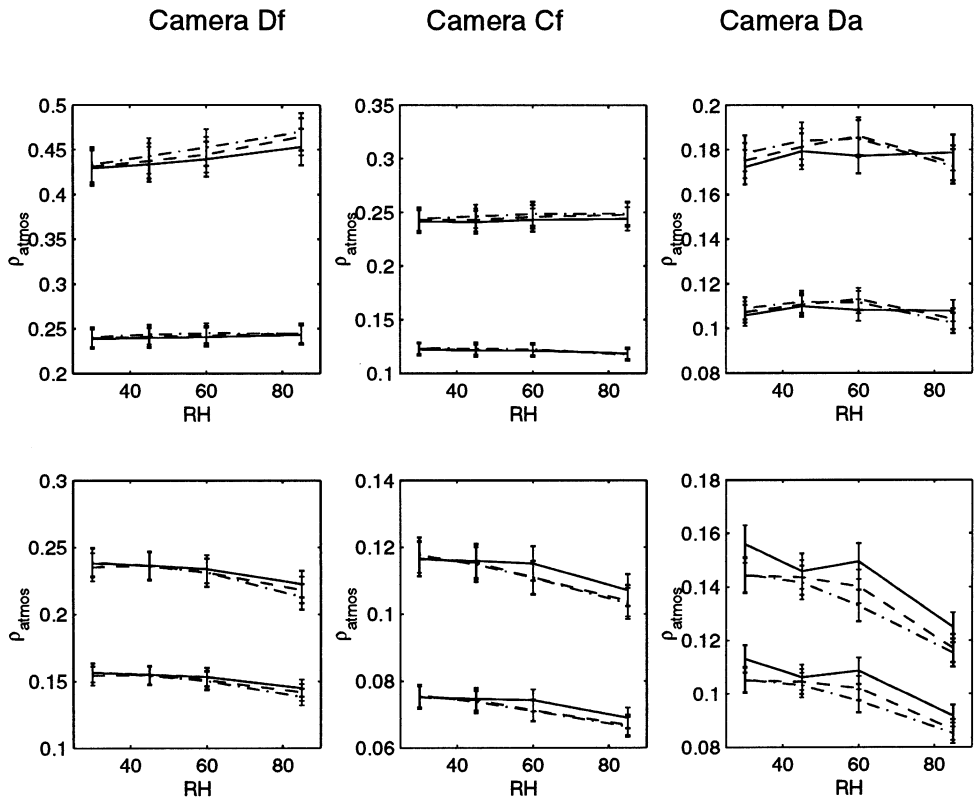

Fig. 12. Atmospheric reflectance (ρ_{atmos}) as a function of the ambient relative humidity for the polluted (top row panels) and clean marine (bottom row panels) aerosol models in the 860 nm band of MISR. Camera Df (forward, 70.5°) is in the 1st column, Camera Cf (forward, 60.0°) is in the 2nd column and Camera Da (behind, 70.5°) is in the 3rd. In each panel, the top group of lines corresponds to $\tau(\lambda = 550\ \text{nm}) = 0.70$ and the bottom 3 corresponds to $\tau(\lambda = 550\ \text{nm}) = 0.30$. The solid line corresponds to a model with $\gamma = 0.4$, dashed line to a $\gamma = 0.6$ and dash-dotted to a $\gamma = 0.8$. The error bars are the nominal calibration uncertainties associated to the band.

ive enough to differentiate reflectances generated by the same aerosol type at different ambient relative humidities. However, the results in the 2100 nm band of MODIS are encouraging (Fig. 11). It is clear that the reflectances are differentiable with respect to the γs for modest optical depths over a wide range of relative humidities. Hence, if the ambient RH can be estimated from the retrieval or by other means, information on the aerosol hygroscopicity can be obtained.

Nevertheless, at this stage, it is unclear if such inversions could be done as routinely as is envisioned for other aerosol parameters by MODIS (Tanré et al., 1997) since there are important practical considerations to be sorted out, namely the non-linear nature of the inversion and whether the pre-flight precision of MODIS in the 2100 nm band can be retained operationally. Also, simulations of the satellite detected radiance must be done with a more comprehensive data set. Although we have used measured aerosol distributions commonly found in different environments, a great part of the data set used here was limited to particles up to 2.50 μm size (diameter) and when data for larger particles was needed, extrapolations of the hygroscopicity had to be made. Thus, our results require further testing with a more comprehensive data set including a better description of aerosols in the size range above 2.50 μm (diameter).

7. Acknowledgements

This research is a contribution to the International Global Atmospheric Chemistry (IGAC) Core Project of the International Geosphere-Biosphere Programme (IGBP) and is part of the IGAC Aerosol Characterization Experiments (ACE). It has been supported by Office of Naval Research Grant N00014-97-1-0132. This is University of Washington JISAO contribution number 652.

REFERENCES

Bluth, R. T., Durkee, P. A., Seinfeld, J. H., Flagan, R. C., Russell, L. M., Crowley, P. A. and Finn, P. 1998. Center for Interdisciplinary Remotely Piloted Aircraft Studies (CIRPAS). *Proceedings of the RPVs 13th International Conference*. RPVs/UAVs. Remotely Piloted Vehicles. Bristol, UK, pp.6/1.10.

Boucher, O. and Anderson, T. L. 1995. General circulation model assessment of the sensitivity of direct climate forcing by anthropogenic sulfate aerosols to aerosol size and chemistry. *J. Geophys. Res.* **100**, 26,117–26,134.

Butler, J.J. and Barnes, R. A. 1998. Calibration strategy for the Earth Observing System (EOS)-AM1 platform. *IEEE Trans. Geosci. Remote Sens.* **36**, 1056–1061.

Carrico, C. M., Rood, M.J. and Ogren, J. A. 1998. Aerosol light scattering properties at Cape Grim, Tasmania, during the First Aerosol Characterization Experiment (ACE-1). *J. Geophys. Res.* **103**, 16,565–16,574.

Carrico, C. M., Rood, M. J. and Ogren, J. A. 2000. Aerosol light scattering properties at Sagres, Portugal, during ACE-2. *Tellus* **52B**, 694–715.

Collins, D. R., Jonsson, H. H., Flagan, R. C., Seinfeld, J. H., Noone, K. J., Öström, E., Hegg, D. A., Gassó, S., Russell, P. B., Livingston, J. M., Schmid, B. and Russell, L. M. 2000. In situ aerosol size distributions and clear column radiative closure during ACE-2. *Tellus* **52B**, 498–525.

Covert, D. S., Charlson, R. J. and Ahlquist, N. C. 1972. A study of the relationship of chemical composition and humidity to light scattering by aerosols. *J. Appl. Meteor.* **11**, 968–976.

Cziczo, D. J., Nowak, J. B., Hu, J. H. and Abbatt, J. P. D. 1997. Infrared spectroscopy of model tropospheric aerosols as a function of relative humidity: observation of deliquescence and crystallization. *J. Geophys. Res.* **102**, 18,843–18,850.

D'Almeida, G. A, Koepke, P. and Shettle, E. P. 1991. *Tropospheric aerosols: global climatology and radiative*. Hampton, Va., USA. A. Deepak Publishers.

Diner, D. J., Bruegge, C. J., Martonchik, J. V., Ackerman, T. P., Davies, R., Gerstl, S. A. W., Gordon, H. R., Sellers, P. J., Clark, J., Daniels, J. A., Danielson, E. D., Duval, V. G., Klaasen, K. P., Lilienthal, G. W., Nakamoto, D. I., Pagano, R. J. and Reilly, T. H. 1989. MISR: a multiangle imaging spectroradiometer for geophysical and climatological research from EOS. *IEEE Trans. on Geosci. Remote Sens.* **27**, 200–214.

Durkee, P. A., Pfeil, F., Frost, E. and Shema, R. 1991. Global analysis of aerosol particle characteristics. *Atmos. Environ.* **25**, 2457–2471.

Durkee, P. A., Jensen, D. R., Hindman, E. E. and Vonder-Haar, T. H. 1986. The relationship between marine aerosol particles and satellite-detected radiance. *J. Geophys. Res.* **91**, 4063–4072.

Durkee, P. A., Nielsen, K. E, Smith, P. J., Russell, P. B., Schmid, B., Livingston, J. M., Holben, B. N., Collins, D., Flagan, R. C., Seinfeld, J. H., Noone, K. J., Öström, E., Gassó, S., Hegg, D., Russell, L. M., Bates, T. S. and Quinn, P. K. 2000. Regional Aerosol Properties from Satellite Observations: ACE-1, TARFOX and ACE-2 results. *Tellus* **52B**, 484–497.

Fitzgerald, J. W. and Hoppel, W. A. 1982. The size and scattering coefficient of urban aerosol particles at Washington, DC as a function of relative humidity. *J. Atmos. Sci.* **39**, 1838–1852.

Fraser, R. S, Kaufman, Y. J. and Mahoney, R. L. 1984. Satellite measurements of aerosol mass and transport. *Atmos. Environ.* **18**, 2577–2584.

Hänel, G. 1976. The properties of atmospheric particles as function of the relative humidity at thermodynamic equilibrium with the surrounding air. *Advances in Geophysics* **11**, 968–976.

Hegg, D. A., Livingston, J., Hobbs, P. V., Novakov, T. and Russell, P. 1997. Chemical apportionment of aerosol column optical depth off the mid-Atlantic coast of the United States. *J. Geophys. Res.* **102**, 25,293–25,303.

Hegg, D. A., Covert, D.S., Rood, M. J. and Hobbs, P. V. 1996. Measurement of the aerosol optical properties in marine air. *J. Geophys. Res.* **96**, 12,883–12,903.

Hansen, J. E. and Travis, L. D. 1974. Light scattering in planetary atmospheres. *Space Sci. Rev.* **16**, 527–610.

Horvath, H., Catalan, L. and Trier, A. 1997. A study of the aerosol of Santiago de Chile (III). Light absorption measurements. *Atmos. Environ.* **31**, 3737–3744.

IGAC. 1995. International Global Atmospheric Chemistry Project, North Atlantic Aerosol Characterization Experiment (ACE-2). *Radiative forcing due to anthropogenic aerosols over the north Atlantic region. Science and implementation plan.* European Commission DG XIII, Report No. CL-NA-16229-EN-C.

Kahn, R., West, R., McDonald, D., Rheingans, B. and Mishchenko, M. I. 1997. Sensitivity of multiangle remote sensing observations to aerosol sphericity. *J. Geophys. Res.* **102**, 16,861–16,870.

Kahn, R., Banerjee, P., McDonald, D. and Diner, D. J. 1998. Sensitivity of multiangle imaging to aerosol

optical depth and to pure-particle size distribution and composition over the ocean. *J. Geophys. Res.* **103**, 32,195–32,214.

Kasten, F. 1969. Visibility in the phase of pre-condensation. *Tellus,* **21**, 631–635.

Kaufman, Y. J. Wald, A. E., Remer, L. A., Bo-Cai, Gao. Rong-Rong, L. and Flynn, L. 1997. The MODIS 2.1 μm channel correlation with visible reflectance for use in remote sensing of aerosol. *IEEE Trans. on Geosci. Remote Sens.* **35**, 1286–1298.

Kiehl, J. T. and Briegleb, B. P. 1993. The relative roles of sulfate aerosols and greenhouse gases in climate forcing. *Science* **260**, 5106, 311–314.

King, M. D., Kaufman, Y. J., Menzel, W. P. and Tanré, D. 1992. Remote sensing of cloud, aerosol, and water vapor properties from the moderate resolution imaging spectrometer (MODIS). *IEEE Trans. on Geosci. Remote Sens.* **30**, 2–27.

Kotchenruther, R. A., Hobbs, P. V. and Hegg, D. A. 1999. Humidification factors for atmospheric aerosol off the mid-Atlantic coast of United States. *J. Geophys. Res.* **104**, 2239–2251.

Kotchenruther, R. A. and Hobbs, P. V. 1998. Humidification factors of aerosol from biomass burning in Brazil. *J. Geophys. Res.* **103**, 32,081–32,089.

Krekov, G. M. 1992. *Models of atmospheric aerosols*. In: Aerosols effects on climate (ed. Jennings, S. G.). The University of Arizona Press, Tucson and London, 9–72.

Li-Jones, X., Maring, H. B. and Prospero, J. M. 1998. The effect of relative humidity on light scattering by mineral dust aerosol as measured in the marine boundary layer over the tropical Atlantic Ocean. *J. Geophys. Res.* **103**, 31,113–31,121.

Lenoble, J. (ed.). 1993. *Atmospheric radiative transfer*, ch. 16. A. Deepak Publishing, Hampton, Virginia, USA.

Nagaraja Rao, C. R., Stowe, L. L. and McClain, E. P. 1989. Remote sensing of aerosols over the ocean using AVHRR data. Theory, practice and applications. *Int. J. Remote Sens.* **10**, 743–749.

Öström, E. and Noone, K. J. 2000. Vertical profiles of aerosol scattering and absorption measured in situ during the North Atlantic Aerosol Characterization Experiment. *Tellus* **52B**, 526–545.

Putaud, J. P., Van Dingenen, R., Mangoni, M., Virkkula, A., Raes, F., Maring, H., Prospero, J. M., Swietlicki, E., Berg, O. H, Hillamo, R. and Makela, T. 2000. Chemical mass closure and origin assessment of the submicron aerosol in the marine boundary layer and the free troposphere at Tenerife during ACE-2. *Tellus* **52B**, 141–168.

Quinn, P. K., Coffman, D. J., Kapustin, V. N., Bates, T. S. and Covert, D. S. 1998. Aerosol optical properties in the marine boundary layer during the First Aerosol Characterization Experiment (ACE-1) and the underlying chemical and physical aerosol properties. *J. Geophys. Res.* **103**, 16,547–16,563.

Raes, F., Bates, T. S., McGovern, F. M. and Van Liedekerke, M. 2000. The second Aerosol Characterization Experiment (ACE-2): general overview and main results. *Tellus* **52B**, 111–126.

Rood, M. J., Shaw, M. A., Larson, T. V. and Covert, D. S. 1989. Ubiquitous nature of ambient metastable aerosol. *Nature* **337**, 537–539.

Saxena, P., Hildemann, L.M., McMurry, P. H. and Seinfeld, J. H. 1995. Organics alter hygroscopic behavior of atmospheric particles. *J. Geophys. Res.* **100**, 18,755–18,770.

Schmid, B., Livingston, J. M., Russell, P. B., Durkee, P. A., Jonsson, H. H., Collins, D. R., Flagan, R. C., Seinfeld, J. H., Gassó, S., Hegg, D. A., Öström, E., Noone, K. J., Welton, E. J., Voss, K., Gordon, H. R, Formenti, P. and Andreae, M. O. 2000. Clear sky closure studies of lower tropospheric aerosol and water vapor during ACE-2 using airborne sunphotometer, airborne in-situ, space-borne, and ground-based measurements. *Tellus* **52B**, 568–593.

Schmeling, M., Russell, L. M., Erlick, C., Collins, D. R., Jonsson, H., Wang, Q., Kregsamer, P. and Streli, C. 2000. Aerosol particle chemical characteristics measured from aircraft in the lower troposphere during ACE-2. *Tellus* **52B**, 185–200.

Stowe, L. L., Ignatov, A. M. and Singh, R. R. 1997. Development, validation, and potential enhancements to the second-generation operational aerosol product at the National Environmental Satellite, Data, and Information Service of the National Oceanic and Atmospheric Administration. *J. Geophys. Res.* **102**, 16,923–16,934.

Swietlicki, E., Zhou, J., Covert, D. S., Hameri, K., Busch, B., Vakeva, M., Dusek, U., Berg, O. H., Wiedensohler, A., Aalto, P., Makela, J., Marinsson, B. G., Papaspiropoulos, G., Mentes, B., Frank, G. and Stratmann, F. 2000. Hygroscopic properties of aerosol particles in the north-eastern Atlantic during ACE-2. *Tellus* **52B**, 201–227.

Tang, I. N. and Munkelwitz, H. R. 1994. Aerosol phase transformation and growth in the atmosphere. *J. Appl. Meteor.* **33**, 791–796.

Tanré, D., Herman, M. and Kaufman, Y. J. 1996. Information on aerosol size distribution contained in solar reflected spectral radiances. *J. Geophys. Res.* **101**, 19,043–19,060.

Tanré, D., Kaufman, Y. J., Herman, M. and Mattoo, S. 1997. Remote sensing of aerosol properties over oceans using the MODIS/EOS spectral radiances. *J. Geophys. Res.* **102**, 16,971–16,988.

Tanré, D., Remer, L. A., Kaufman, Y. L., Mattoo, S., Hobbs, P. V., Livingston, J. M., Russell, P. B. and Smirnov, A. 1999. Retrieval of aerosol optical thickness and size distribution off the mid-Atlantic coast of the United States. *J. Geophys. Res.* **104**, 2261–2278.

Vermote, E. F., Tanré, D., Deuzé, J. L., Herman, M. and Mocrette, J. J. 1997. Second simulation of the satellite signal in the solar spectrum, 6S: an overwiev. *IEEE Trans. Geosci. Remote Sens.* **35**, 3, 675–686.

Verver, G., Raes, F., Vogelezang, D. and Johnson, D.

2000. The second Aerosol Characterization Experiment (ACE-2): meteorological and chemical context. *Tellus* **52B**, 126–140.

World Climate Programme. WCP-112. 1986. *A preliminary cloudless standard atmosphere for radiation computation.* WMO/TD-No. 24, Geneva.

Waggoner, A. P., Weiss, R. E., Ahlquist, N. C., Covert, D. S., Will, S. and Charlson, R. 1984. Optical characteristics of atmospheric aerosols. *Atmos. Environ.* **15**, 1891–1909.

Zhang, X. Q., McMurry, P. H., Hering, S. V. and Casuccio, G. S. 1993. Mixing characteristics and water content of submicron aerosols measured in Los Angeles and at the Grand Canyon. *Atmos. Environ.* **27**, 1593–1607.